

ORIGINAL ARTICLE

Open Access



# Comparative Study of the Rock-breaking Mechanism of a Disc Cutter and Wedge Tooth Cutter by Discrete Element Modelling

Hua Jiang<sup>1</sup>, Huiyan Zhao<sup>1</sup>, Xiaoyan Zhang<sup>1,2\*</sup>, Yusheng Jiang<sup>1</sup> and Yaofu Zheng<sup>1</sup>

## Abstract

The operation of a shield tunnel boring machine (TBM) in a high-strength hard rock stratum results in significant cutter damage, adversely affecting the thrust and torque of the cutter head. Therefore, it is very important to carry out the research on the stress characteristics and optimize the cutter parameters of cutters break high-strength hard rock. In this paper, the rock-breaking performance of cutters in an andesite stratum in the tunnel of Qingdao Metro Line No. 8 was investigated using the discrete element method and theoretical analysis. The rock-breaking processes of a disc cutter and wedge tooth cutter were simulated by software particle flow code PFC<sup>3D</sup>, and the rock-breaking degree, stress of the cutter, and rock-breaking specific energy were analyzed. The rock damage caused by the cutter in a specific section was divided into three stages: the advanced influence, crushing, and stabilizing stages. The rock-breaking degree and the tangential and normal forces of the wedge tooth cutter are larger than that of the disc cutter under the same conditions. The disc cutter (wedge tooth cutter) has the highest rock-breaking efficiency at a cutter spacing of 100 mm (110 mm) and a penetration depth of 8 mm (10 mm), and the rock-breaking specific energy is 11.48 MJ/m<sup>3</sup> (12.05 MJ/m<sup>3</sup>). Therefore, two types of cutters with different penetration depths or cutter spacing should be considered. The number of teeth of wedge tooth cutters can be increased in hard strata to improve the rock-breaking efficiency of the shield. The research results provide a reference for shield cutterhead selection and cutter layout in similar projects.

**Keywords** Qingdao andesite, Rock breaking with cutter, Wedge tooth cutter, Specific energy, PFC<sup>3D</sup>

## 1 Introduction

TBM has become the preferred construction method for developing underground urban areas. Delisio et al. [1] obtained the relationship between rock mass conditions and TBM performance based on blocky rock masses and field permeability index (FPI). Hassanpour et al. [2] compiled and analyzed the actual machine performance database of different hard rock TBM tunneling projects

to develop a new TBM performance prediction model. Yagiz et al. [3] assessed the impact of rock mass properties on TBM performance and constructed a new empirical equation to estimate TBM performance. The database is built using data collected from hard rock TBM tunnel. Gong et al. [4] established a statistical prediction model of TBM penetration rate based on the tunneling process of TBM in hard rock. The above studies are based on different methods to predict TBM performance under hard rock conditions. Although they have certain limitations, they can provide a reference for projects with similar formation conditions.

In the current experimental research on rock breaking with cutters, the relatively more widely used instrument is linear cutting testing machine [5–8]. With this

\*Correspondence:

Xiaoyan Zhang  
zhangxiaoyan@cumtb.edu.cn

<sup>1</sup> School of Mechanics and Civil Engineering, China University of Mining and Technology, Beijing 100083, China

<sup>2</sup> Beijing Urban Construction Group Co., Ltd., Beijing 100088, China

instrument, different parameters such as cutter penetration, cutter spacing and force can be set. Smith et al. [9] explored the influence of the supportive relationship between the rock contacted by the TBM tool and the surrounding rock on the excavation performance of a TBM and proposed suggestions. Innaurato et al. [10, 11] developed an indenter test to simulate the effect of the disc cutter on the rock specimen on a roadway working face. The results showed that the thrust increment required to destroy the rock between the indenter and the free surface of the specimen had a negligible influence on the restraint stress. Yang et al. [12] conducted a micro-cutter head test on sandstone rock to analyze the influence of the inclination and spacing on the crushing efficiency of the TBM and the rock cracking behavior. Lin et al. [13] analyzed the crack propagation and failure modes of intact rock and jointed rock under different confining pressures by a triaxial testing machine. Entacher et al. [14] conducted full-scale cutting tests to evaluate the global energy input compared to rock debris and excavation volume. Compared with theoretical formula calculation and analysis or numerical simulation, the test process is closer to the actual engineering situation and the test results are more intuitive. But at the same time, there are also some disadvantages, such as a long test cycle, consuming manpower and material resources.

At present, the discrete element method (DEM) is widely used in the numerical simulation of cutter rock breaking process [15–18]. PFC<sup>3D</sup> can simulate relatively complex motion patterns such as the cutter cutting process, and the overall effect is better [19, 20]. Choi et al. [21] studied the relationship between the rock fracture mechanism and the orientation and spacing of rock joints and fractures using numerical software. Gong et al. [22, 23] used the DEM to perform two-dimensional numerical simulations to explore the influence of the joint orientation and spacing on rock fragmentation by a TBM cutter. Cho et al. [24] carried out a series of numerical experiments to simulate the rock fragmentation of the TBM disc cutter and used AUTODYN-3D to simulate the three-dimensional dynamic failure observed in the linear cutter test by linear cutter machine (LCM). In the research of rock breaking with a cutter by numerical simulation, the main content of researchers usually is to change the relevant setting parameters of cutter under certain rock parameters, such as the distance between two cutters, the shape and size of the cutter itself, and the penetration rate of the cutter in rock. By changing these parameters, we can further study the force change law of the cutter and the law of rock fragmentation.

Many researchers [25–27] regard the specific energy of rock breaking, that is, the energy consumed to cut and destroy the unit volume of rock, as the indicator of rock

breaking efficiency. Zhang et al. [28] analyzed the rock-breaking mechanism of a TBM under traditional working conditions and on a free surface. The results showed that the crushed rock particles were larger under free-surface than under traditional working conditions. Mohammadnejad et al. [29] conducted scratch tests to evaluate the tool's cutting speed, cutting angle, and cutting depth. The results showed that this method was advantageous for capturing the fracture mechanism of the rock and the tool cutting performance. Xia et al. [30] studied the mechanism and changes in the lateral force of the TBM's center cutter. The study showed that the inside of the center milling cutter formed a transverse rolling ring gap in the rock during rotary cutting. The smaller the installation radius, the greater the tool's lateral force was. Rostami [31] analyzed the pressure distribution during the cutting process of different rock types using on-site data and a new abrasiveness test method (NAT). It was found that the pressure in the contact area was more concentrated and the compressed area was smaller than that predicted by a previous model. At present, various research institutions or researchers have adopted the method of theoretical calculation combined with numerical simulation or theoretical analysis combined with experimental research to research the rock breaking theory of cutter. The research on the rock-breaking theory of the cutter is conducive to further studying the interaction between the cutter and rock in the field shield tunneling process, improving the shield tunneling efficiency, and improving the rock-breaking effect of the cutter.

Andesite is a common stratum type in the Qingdao subway area. This rock type has resulted in severe damage to the disc cutters during shield tunnel construction in many subway lines. We use the shield project of the Qingdao Metro Line 8 as an example. With the help of the advantage of three-dimensional discrete element software PFC<sup>3D</sup> in simulating cutter rock breaking, the simulation of the cutting process of cutter rotation and revolution is added on the basis of the two-dimensional numerical model to study the impact of the cutter on rock breaking efficiency under different penetration and cutter spacing conditions in andesite formation. Since both disc cutters and wedge tooth cutters are used in a shield machine, we compare the cutters' rock-breaking efficiency and characteristics in an andesite stratum to provide a reference for cutter design and efficient rock breaking and tunneling using a shield TBM under similar stratum conditions as those in the Qingdao Metro.

## 2 Background

This study considers the "Citizen fitness center station to Guantao station" section of the Qingdao Metro Line 8. The shield passes through slightly weathered tuff

and slightly weathered andesite strata with high rock strength. Excessive thrust and torque of the cutterhead often occur during shield propulsion and represent challenges in shield construction. The geological profile of the area surrounding the tunnel is shown in Figure 1. We focus on the interaction between the cutter and the rock in the slightly weathered andesite stratum. A 7-m shield machine is used during shield construction. The cutter head has 4 main spokes and 8 pairs of spokes. The opening rate is 35%, which results in sufficient strength and stiffness. The rock-breaking capacity of the cutter head is 150 MPa. The cutter has 49 blades, 8 double-edge cutters and 33 single-edge cutters. The cutter has a 432-mm single-edge cutter ring.

In the early stage of shield construction, the cutters on the cutter head are typically disc cutters. After a certain distance had been excavated, it was discovered that the thrust and torque of the shield cutter head were extremely high. It was found that the cutter was damaged and showed excessive wear, as shown in Figure 2, resulting in low rock-breaking efficiency. As a result, frequent tool changing was required, reducing the construction efficiency and threatening the safety of the workers. Therefore, during the middle to late stages of shield tunneling, the disc cutter was replaced with a wedge tooth cutter to enhance the efficiency of shield tunneling.

However, the tunneling parameters (such as penetration rate, cutter spacing) setting for wedge cutters is based on the experience of disc cutters which may not optimize the cutting efficiency. Therefore, it is very important to carry out the comparative study of wedge cutter and disc cutter by numerical simulation, optimize the tool combination layout and optimize the tunneling parameters to improve the tunneling efficiency.

### 3 Establishment of Particle Flow Model

#### 3.1 Calibration of Micro Parameters

Software PFC<sup>3D</sup> by combining independent particles through a parallel bond model (PBM) to simulate the mechanical behavior of continuum materials, such as rock. The PBM can be regarded as a series of springs with normal and tangential stiffness, which are uniformly distributed on the contact surface with a certain width to resist the force and torque simultaneously. In the PBM, the failure of a bond results in an immediate reduction in the macroscopic stiffness, which represents the brittle failure characteristics of hard rock. Therefore, PBM was selected to simulate the mechanical behavior of hard rock during failure. The mesoscopic parameters of the PBM include the effective bond modulus  $E_c$ , the ratio of normal to shear stiffness  $k_n/k_s$ , the friction coefficient between

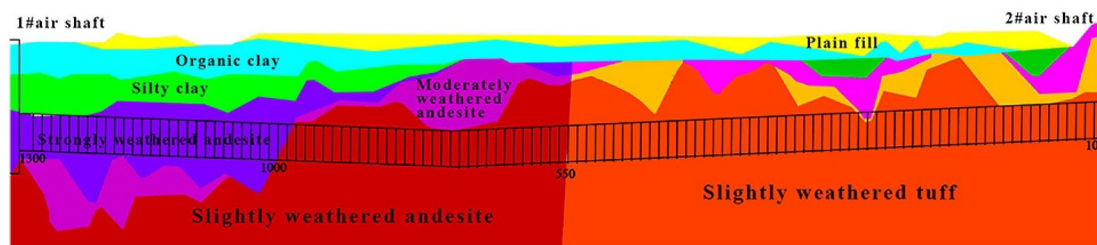


**Figure 1** Geological profile for the section of "Citizen fitness center station to Guantao station" of Qingdao Metro Line 8

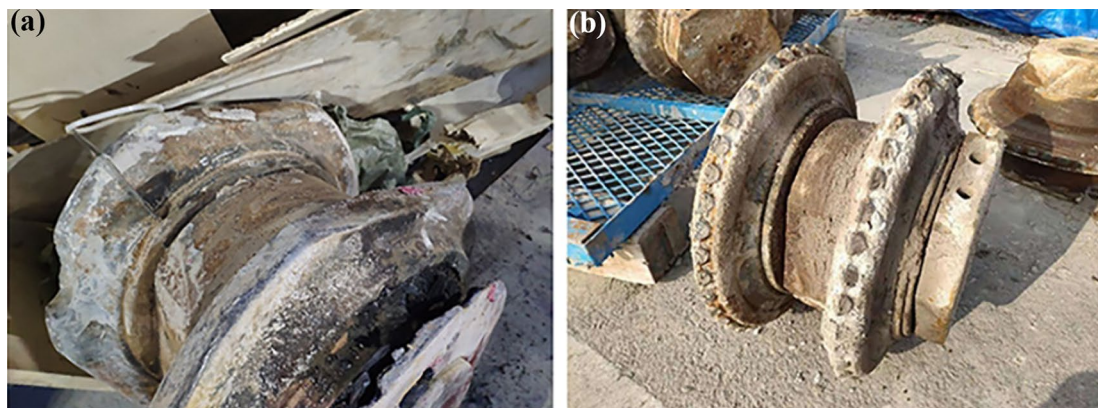


**Figure 2** Disassembled cutter wear and damage diagram: **a** Wear of disc cutter, and **b** Damage of wedge tooth cutter

particles  $\mu$ , the normal strength of parallel bonding  $\sigma$ , and shear strength  $\tau$ .

Many scholars have made detailed research on PFC parameter calibration [32–35]. Based on the above research, the rules are summarized as follows. The main meso-parameters affecting the elastic modulus were  $E_c$  and  $k_n/k_s$ . The elastic modulus was positively correlated with  $E_c$  and negatively correlated with  $k_n/k_s$ . Many meso-parameters affect the compressive strength, including  $k_n/k_s$ ,  $\sigma$ , and  $\tau$ . The compressive strength increased and then decreased with the  $k_n/k_s$ , whereas the main meso-parameters of the PBM ( $\sigma$  and  $\tau$ ) were positively correlated with the compressive strength.

The micro-properties were calibrated by modeling the uniaxial compressive strength (UCS) test in PFC<sup>3D</sup>. UCS model was a 50 mm×100 mm cylinder. We established the upper and lower loading plates and a cylindrical surface as the boundaries and then generated particles in the

enclosed area of the three surfaces. The particle radius is 3–4.5 mm. As shown in Figure 3. We used the Fishtank command in the PFC<sup>3D</sup> program to compact the particles by applying stress to the walls to represent the macroscopic state of the rock. A loading speed was applied to the upper and lower planes, and the specimen was subjected to a force to destroy it by slow pressure.

During the calibration process, the micro-properties were varied systematically by using the trial and error method. The axial stress vs. axial strain curves were plotted after each trial and checked whether the curves exhibit macro-properties or not. It was repeated until the response of the model achieved a good agreement with the response of the rock sample. The strength curve and model after calibration of uniaxial compression test are shown in Figure 4. The results of the calibration parameters are shown in Table 1.

### 3.2 Establishment of Rock and Cutter Model

The TBM cutter breaks the rock using a circular motion. If the size of the rock mass is too large, the number of particles is very large, significantly

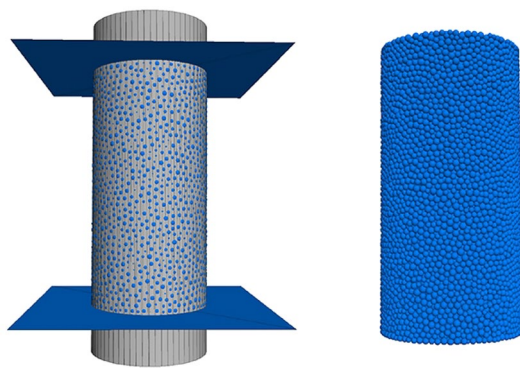


**Figure 3** Uniaxial compression test model

**Table 1** Micro-parameters obtained from the calibration process

Micro-parameters	Value
Effective bond modulus $E_c$ (GPa)	36
Ratio of normal to shear stiffness $k_n/k_s$	2.0
Friction coefficient between particles $\mu$	0.5
Normal strength $\sigma$ (MPa)	120
Shear strength $\tau$ (MPa)	120

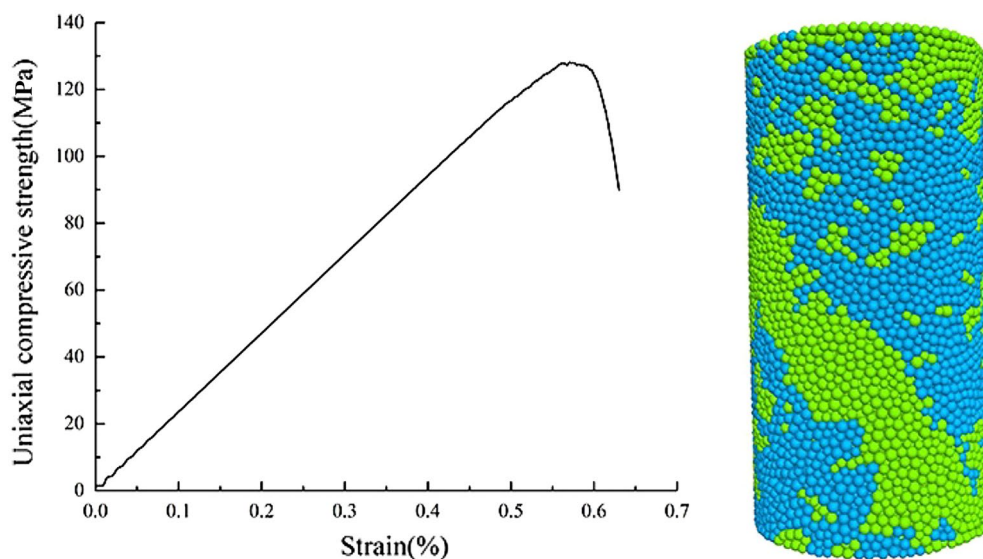


**Figure 4** Strength curve and model after calibration in uniaxial compression test



increasing the simulation duration. Thus, it is necessary to simplify the model. A section of the arc was selected as the rock mass broken by the cutter. The inner diameter of the arc was 450 mm, the outer diameter was 1000 mm, and the angle of the center of the arc was  $60^\circ$ . The particle radius used in the numerical simulation calculation is 3–4.5 mm, the number of particles is 205661, and the number of surface units is 1106.

In order to make the simulated state of the model approximate to the actual state, the initial equilibrium state of the model needs to be solved. Set boundary wall constraints around and at the bottom of the model, and add a gravity field. The initial balance between particles and between particles and walls is specified as a linear stiffness contact model. When the model reaches the initial equilibrium, the linear stiffness contact model between particles is replaced by the parallel bond model, and the new contact model is given with constitutive parameters. After the equilibrium is calculated again, the sand-gravel stratum model with the same physical and mechanical properties as the actual stratum required for numerical calculation is obtained. The rock model is shown in Figure 5.

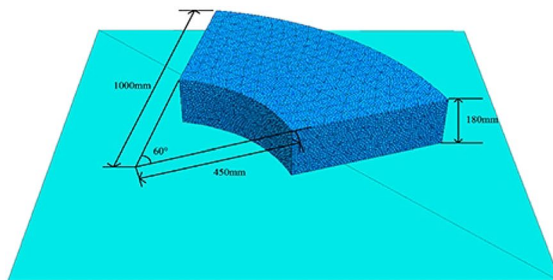


**Figure 5** Rock model diagram

The size of the disc cutter was 432 mm. The wedge tooth cutter had the same size and 40 teeth. The cutter used in the TBM is shown in Figure 6, and the cutter model established in PFC<sup>3D</sup> software is shown in Figure 7. The cutter model is completely rigid.

The layout of the shield cutter significantly affects the rock-breaking efficiency during construction. Therefore, we evaluated the effect of different cutter spacings and penetration depths on the number of particles/cracks in a given section, the cutter force, and the specific energy of rock breaking to determine the optimal rock-breaking parameters. The range of the cutter spacing of the actual shield cutter is 80–120 mm. Thus, we evaluated five cutter spacings (80 mm, 90 mm, 100 mm, 110 mm, and 120 mm) and three penetration depths (10 mm, 8 mm, and 6 mm) in the numerical simulation of the disc cutter and the wedge tooth cutter.

## 4 Three-Dimensional Numerical Simulation Analysis

### 4.1 Simulation Process and Data Recording

We use the disc cutter as an example to describe the rock-breaking simulation based on actual conditions, i.e., the cutter has a circular motion. Due to the layout design



**Figure 6** Cutters used in the field: **a** Disc cutter, and **b** Wedge tooth cutter

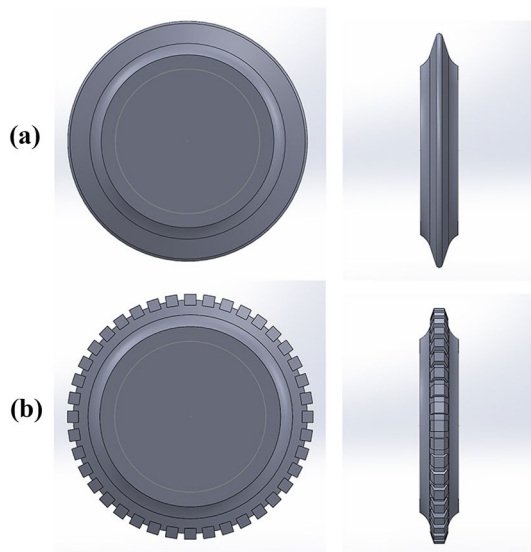


**Figure 7** Established cutter model in numerical simulation: **a** Disc cutter model, and **b** Wedge tooth cutter model

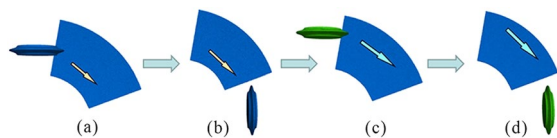


**Figure 8** Rock-breaking process of disc cutter: **a** Rock-breaking start of #1 cutter, **b** End of rock-breaking by #1 cutter, **c** Rock-breaking start of #2 cutter, and **d** End of rock-breaking by #2 cutter

of the head cutter, the first cutter and the second cutter operate sequentially during rock breaking; thus, the simulation uses two cutters. A diagram of the rock-breaking process of the disc cutter with a cutter spacing of 100 mm is shown in Figure 8. The simulation process of the wedge tooth cutter is the same.

The initial position of the cutter is at the outer circumference of the rock model. There is a small distance between the initial position and the rock mass to ensure to prevent interaction between the cutter and the rock mass in the initial stage. The cutter rotates around the center axis until there is no contact force with the rock; then, the rotation is terminated. During the rock-breaking simulation, a cycle command is used to customize the calculation times of each cutter. The calculation times are equal to the traveling distance of the cutter. In addition to the angular velocity of the cutter rotating around the origin, the angular velocity of the cutter rotation around its central point is defined to simulate the movement of the rock-breaking cutter in the field. The normal force and tangential force on the wall surface of the cutter are recorded using the wall history command.

In addition to recording the contact force between the cutter and the rock, the rock-breaking performance of the cutter is determined. Rock crushing results in broken particles and cracks between particles. The number of broken particles is obtained by looking at the particle group grouping. The number of fractures can be obtained by looking at the particle fractures group. The green particles indicate the compression failure of particles, and the red particles indicate the tensile failure of particles. Cracks form between particles due to particle fragmentation. PFC<sup>3D</sup> models particles as balls, and the cracks between the particles are represented by disks. Thus, a disk is formed between two particles when a crack occurs, and the number of cracks reflects the degree of damage.

#### 4.2 Analysis of Rock-Breaking Process of Cutter

A vertical section is selected at 30° to observe the rock-breaking efficiency of the cutter during rock breaking.

We use a cutter spacing of 100 mm and a penetration depth of 8 mm scheme as an example. The failure of the particles in a cross-section is recorded when the #1 and #2 cutters roll 15°, 30°, 45°, and 60°. The results are shown in Tables 2, 3 and Figure 9.

The results of the disc cutter show that when the 1# cutter rolls to 15°, minimal damage occurs in the section before the cutter reaches the selected section. There are 2 broken particles in the section; one particle experienced compression failure, and the other suffered tension failure. This stage is called the advanced influence stage. When the 1# cutter rolls to 30°, the cutter reaches the selected section, and the number of broken particles increases to 36, with 21 particles with compression failure and 15 particles with tensile failure. The disturbance of the #1 cutter causes some damage to the surrounding rock. This is called the crushing stage. As the #1 cutter rolls to 45° and 60°, it has passed the selected section, and the number of broken particles in the section stabilizes. This is called the stabilizing stage.

After the #1# cutter has broken the rock, the #2 cutter begins to roll. The damage of the #2 cutter to the section also goes through three stages. As the #2 cutter operates, the damage degree in the cross-section increases and reaches the maximum at about 30°. At this time, there are 86 broken particles, of which 48 were broken by the #2 cutter, and 38 were broken by the #1 cutter. As the #2 cutter continues to operate, the damage to the section stabilizes. The number of rock particles damaged by the #2 cutter is greater than that of the #1 cutter due to the small distance between the two cutters. Thus, there is existing damage caused by the #1 cutter when the #2 cutter operates in the same area.



Table 2 Failure of the disc cutter in section

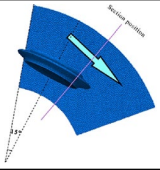
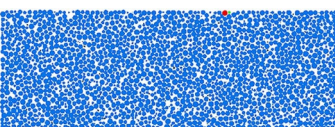
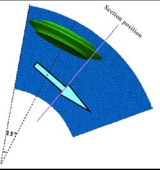
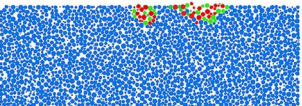
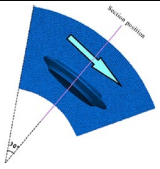
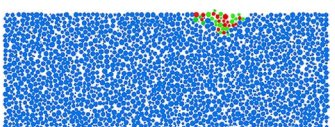
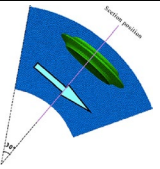
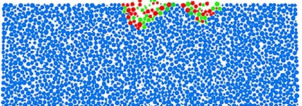
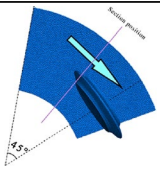
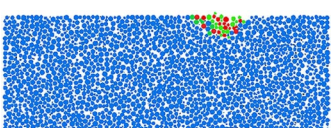
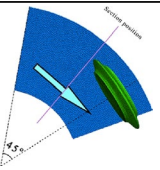
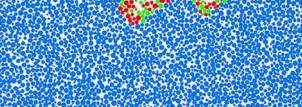
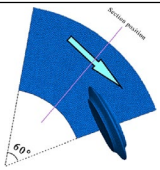
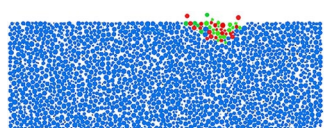
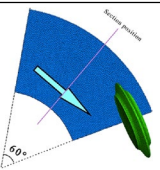
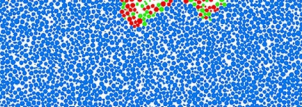
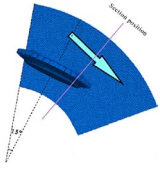
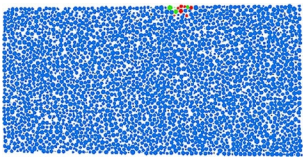
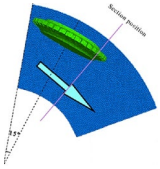
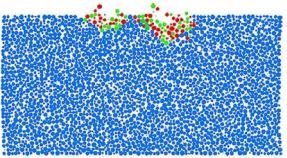
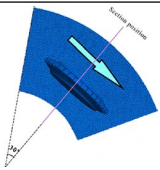
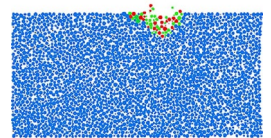
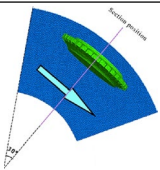
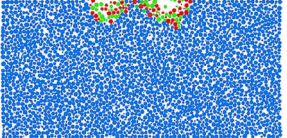
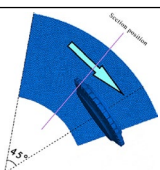
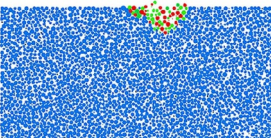
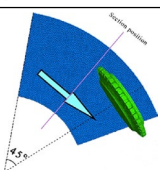
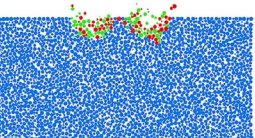
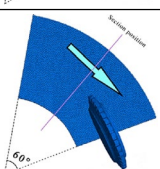
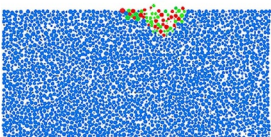
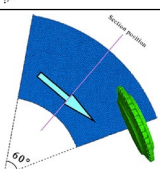
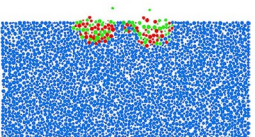
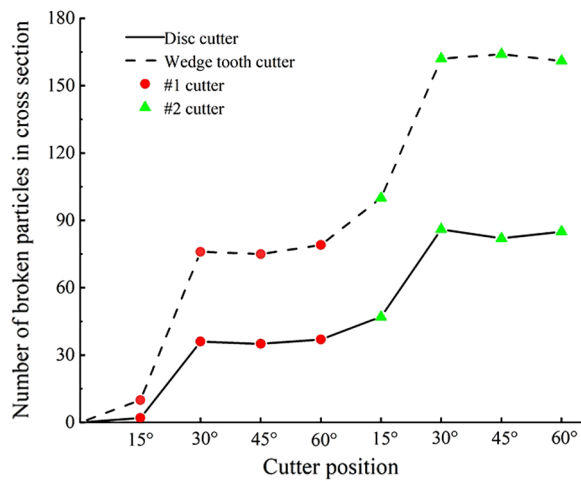
Cutter position (#1 cutter)	Failure in section	Cutter position (#2 cutter)	Failure in section
			
			
			
			

Table 3 Failure of the wedge tooth cutter in section

Cutter position (#1 cutter)	Failure in section	Cutter position (#2 cutter)	Failure in section
			
			
			
			



**Figure 9** Cutter position and section particle failure diagram

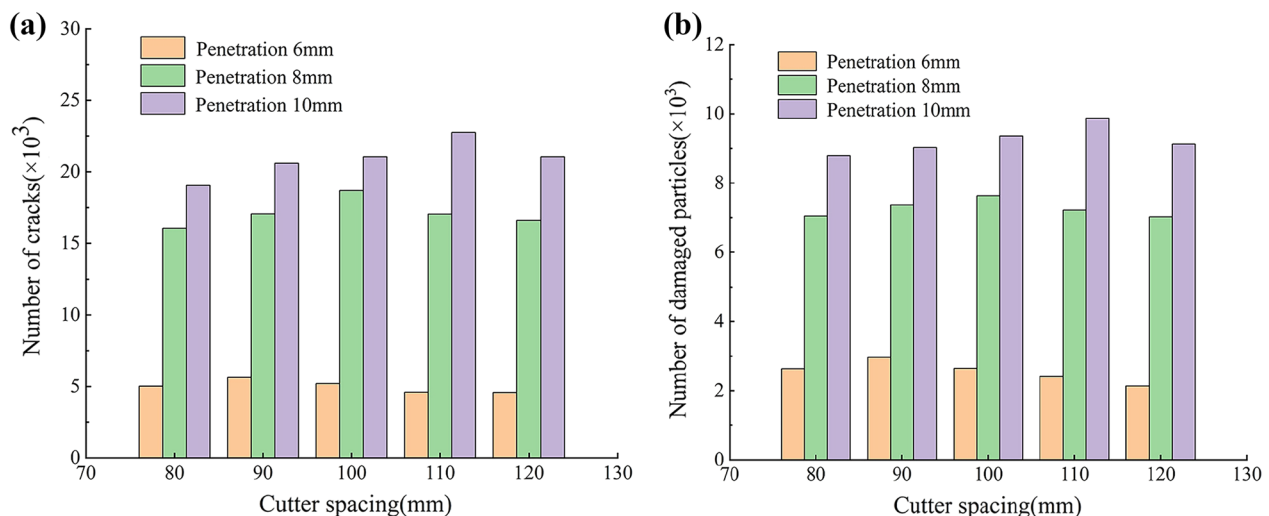
The rock-breaking process is similar for the wedge tooth cutter and the disc cutter and is not discussed here. When the wedge tooth cutter reaches 30°, there are 162 broken particles in the cross-section, compared with 86 broken particles for the disc cutter under the same conditions. Thus, the wedge tooth cutter is more destructive than the disc cutter. Due to the large degree of rock damage caused by the wedge tooth cutter, overlap exists in the rock-breaking area of the two cutters; thus, repeated rock breaking occurs between the two cutters.

### 4.3 Analysis of Rock Fragmentation for Different Penetration Depths and Cutter Spacing

#### 4.3.1 Disc Cutter

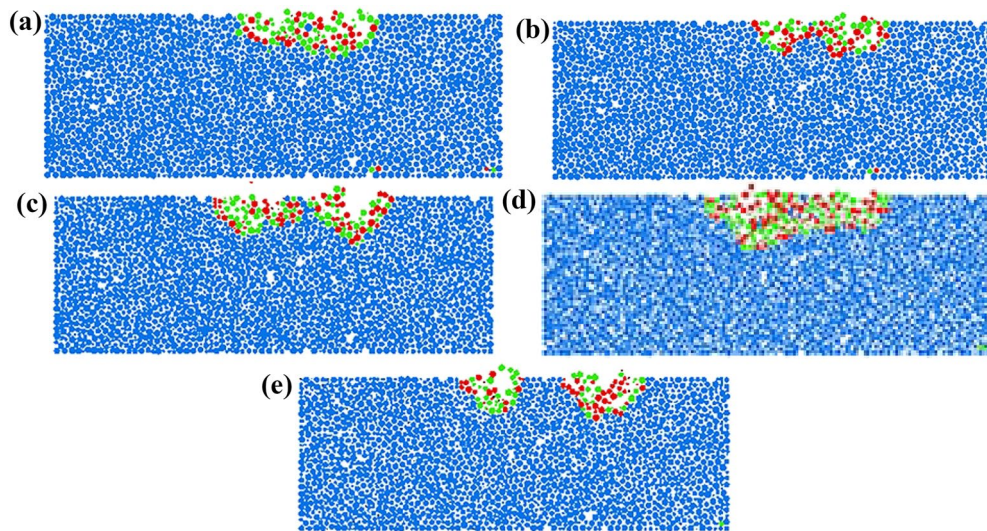
Figure 10 shows that the number of cracks and broken particles in the rock increases with an increase in the cutter's penetration depth for the same cutter spacing, indicating that a greater penetration depth results in greater rock fragmentation. When the penetration depth is constant, the number of cracks and broken particles follows a parabolic trajectory as the distance between the two cutters increases. There is an upward trend because of an overlap in the rock-breaking area of the two cutters when the cutter spacing is small, resulting in the repeated breaking of the rock between the two cutters. As the distance between the cutters increases, the overlap in the broken area decreases, and the degree of rock fragmentation increases. After reaching the maximum distance between the cutters, the damage to the rock by the cutter decreases; thus, the number of cracks and broken particles declines.

Figure 11 shows the rock-breaking profile of the cutters with different cutter spacings for a penetration depth of 10 mm. As the cutter spacing increases, the transverse range of the red and green areas (broken areas) increases, the blue area (undamaged area) between the #1 and #2 cutters increases, and the overlap in the two cutters' rock-breaking area decreases. The numbers of cracks and particles reach the peak at a cutter spacing of 110 mm, and at a cutter spacing of 120 mm, there is no more overlap in the fracture zone between the two cutters, and no penetrating cracks are generated.



**Figure 10** Statistics of particles and cracks at the end of rock breaking with 2 # disc cutter: **a** Variation of crack number in different cutter spacing of disc cutter, and **b** Variation of the number of damaged particles in different cutter spacing of disc cutter





**Figure 11** Under the condition of penetration 10 mm, the rock-breaking profile of disc cutter with different cutter spacing: (a) Cutter spacing 80 mm, (b) Cutter spacing 90 mm, (c) Cutter spacing 100 mm, (d) Cutter spacing 110 mm, and (e) Cutter spacing 120 mm

The rock breaking profile of the cutter with different penetration depths for a 100 mm cutter spacing is shown in Figure 12. The results are similar to those in Figure 11, i.e., the depth of the rock fragmentation area increases with an increase in the penetration depth.

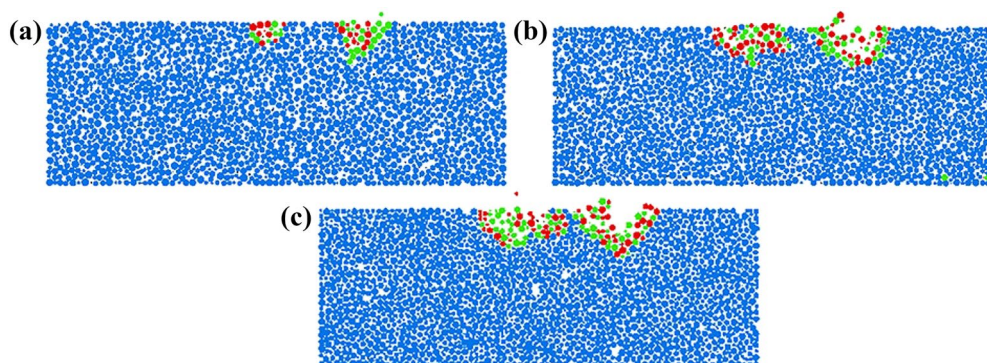
#### 4.3.2 Wedge Tooth Cutter

Figure 13 shows that the results are similar to those of the disc cutter for a constant distance between the two cutters. For constant penetration depths of the cutter (6 mm, 8 mm), the number of cracks and broken particles follows a parabolic trajectory as the distance between the two cutters increases. However, the number of cracks and broken particles in the rock shows an upward trend for a penetration depth of 10 mm, indicating no overlap between the two cutters. The rock damage degree caused by the wedge tooth cutter is greater than that of the disc

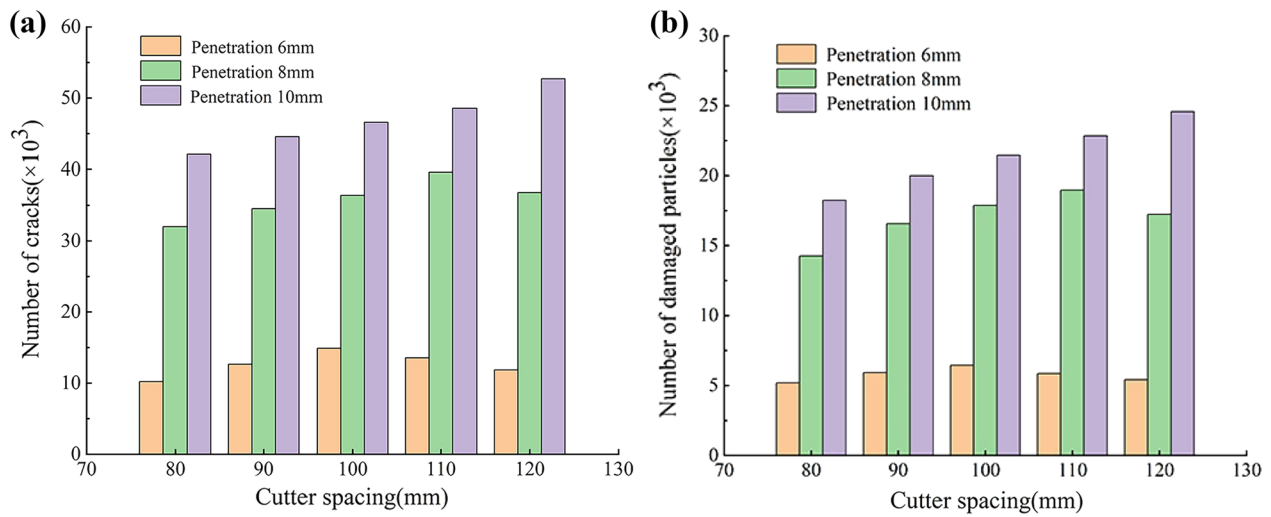
cutter because of the larger number of cracks and broken particles.

Figure 14 shows the rock-breaking profile of the cutters with different cutter spacings for a 10 mm penetration depth. As the cutter spacing increases, the transverse range of the red and green areas (broken areas) increases, the blue area (undamaged area) between the #1 and #2 cutters increases, and the overlap between the two cutters' rock-breaking areas decreases.

Figure 15 shows the rock-breaking profile of the wedge tooth cutter with different penetration depths for a 100 mm cutter spacing. The rock-breaking process is relatively stable at a penetration depth of 6 mm. However, greater breakage occurs at the bottom of the cutting path at a penetration depth of 8 mm, and penetration cracks occur at 10 mm, in addition to an increase in the rock-breaking area at the bottom. These results show that



**Figure 12** Under the condition of cutter spacing 100 mm, the rock-breaking profile of disc cutter with different penetration: a Penetration 6 mm, b Penetration 8 mm, and c Penetration 10 mm



**Figure 13** Statistics of particles and cracks at the end of rock breaking with 2 # wedge tooth cutter: **a** Variation of crack number in different cutter spacing of wedge tooth cutter, and **b** Variation of the number of damaged particles in different cutter spacing of wedge tooth cutter

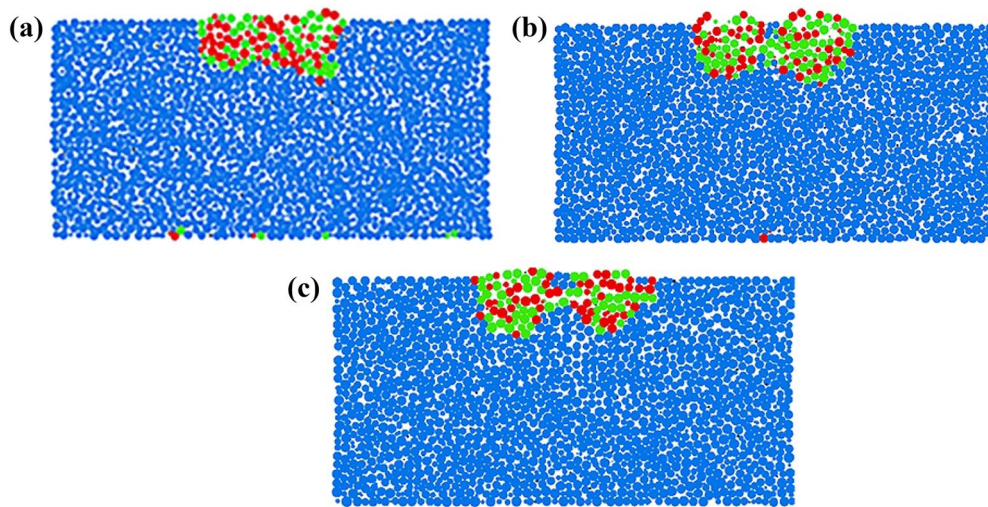


**Figure 14** Under the condition of penetration 10 mm, the rock-breaking profile of disc cutter with different cutter spacing: **a** Cutter spacing 100 mm, **b** Cutter spacing 110 mm, and **c** Cutter spacing 120 mm

the wedge tooth cutter is more destructive than the disc cutter.

#### 4.4 Analysis of the Cutter Force in Different Schemes

##### 4.4.1 Force Analysis of Disc Cutter

The normal force and tangential force of the #1 and #2 cutters are extracted for 100 mm cutter spacing and 8 mm penetration depth. The results are shown in Figure 16. The calculation time step is equivalent to that in the numerical simulation and is proportional to the rock-breaking distance of the cutter.

Figure 16(a) and (b) shows that the tangential force and normal force of the #1 and 2# cutters fluctuate with an

increase in the calculation time step during rock cutting. As shown in Figure 16(a), the tangential force and the fluctuation range are relatively large after rock cutting by the #1 cutter. When the #2# cutter cuts on the given path with a 100 mm cutter spacing, the fluctuation amplitude of the tangential force on the cutter and the average tangential force decrease. This result is attributed to the partial overlap between the breaking areas of the two cutters, that is, the 1 # cutter has pre-broken some rocks, reducing the force on the 2 # cutter, which is conducive to the cutting of the 2 # cutter on rocks. Figure 16(b) indicates that the change in the normal force of the cutter is greater than that of the tangential force. The normal



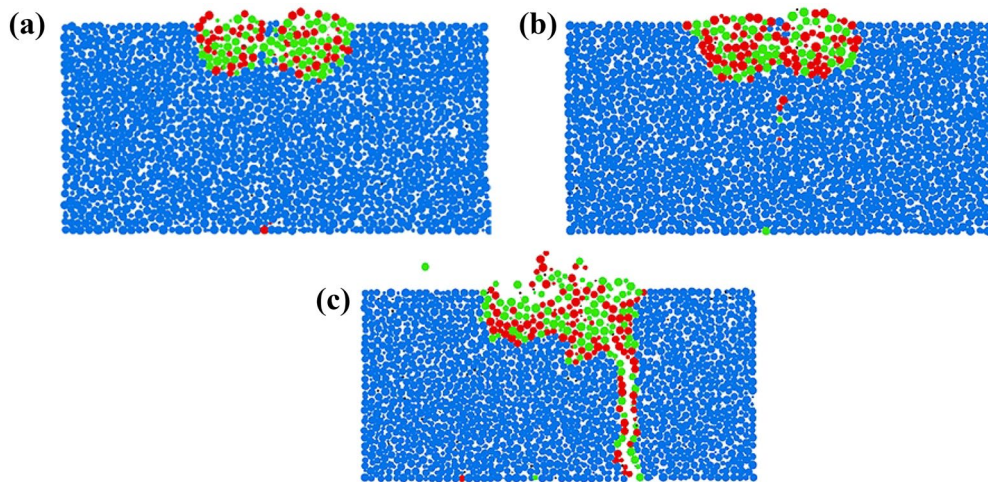


**Figure 15** Under the condition of cutter spacing 100 mm, the rock-breaking profile of disc cutter with different penetration: **a** Penetration 6 mm, **b** Penetration 8 mm, and **c** Penetration 10 mm

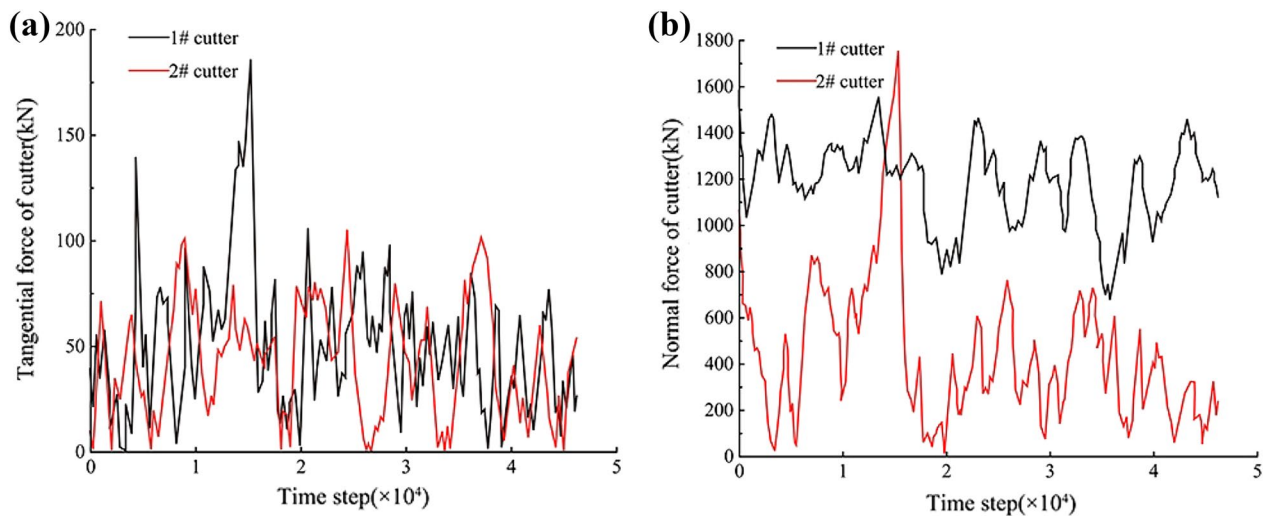


**Figure 16** Force change diagram of disc cutter: **a** Variation diagram of tangential force of disc cutter, and **b** Variation diagram of normal force of disc cutter

force of the #1 cutter is always higher than that of the #2 cutter due to the overlap. Thus, the #2 cutter requires less force to break the rock.

The normal force and tangential force of the cutter show a fluctuating trend, sharply increasing and then decreasing. The reason is that the rock is gradually crushed and cracked by the cutter. The rock under the blade is crushed first, and the force of the cutter increases as it penetrates the rock on both sides, resulting in lateral cracks. As the lateral cracks expand and particles separate from the main rock mass, the vertical thrust of the cutter decreases suddenly. Subsequently, the cutter continues to push forward, and the vertical thrust increases again,

resulting in the fluctuation of the vertical thrust. As the rock is broken and particles are generated, the penetration depth of the cutter increases. When the blade of the cutter has penetrated sufficiently, the whole rock mass is broken, and rock particles between the two adjacent cutters fall off due to the intersection of cracks. In summary, when the cutter penetrates into the rock, the rock failure consists of numerous small and large damage events. When the rock is penetrated and broken by the cutter, the cutter moves forward, breaking more rock.

The rock contact force chain reflects the contact force between the particles. The shape of the force chain is cylindrical; the color of the cylinder represents different



forces, and the thickness of the cylinder represents the size of the force. Figure 17 shows two types of contact forces in the numerical simulation results: the pulling force (white) and the pressure (blue). The two grooves in the middle are formed by the two cutters. Since the particles in the middle of the grooves have been destroyed, there is no contact force, and the grooves are empty. The dominant contact force at the bottom of the cutter is pressure, and there is a radial extension at the bottom, indicating that part of the pressure contact force has been transferred below. A small pressure contact force occurs at the bottom of the rock because the wall limits its displacement, resulting in compression of the rock at the bottom. The contact force cylinder near the outside of the rock is very thin, indicating the propagation of the contact force into the rock. The cylinder is thicker where the cutter touches the rock because the pulling force is

larger, indicating that the dominant internal contact force of the rock is tensile force. It should be noted that the continuity of the pressure chain of the right cutting track is better than that of the left cutting track because the surrounding rock particles are disturbed by the first cutter, and the size of the particles is variable, resulting in an irregular removal of the rock particles on the left side of the cutter. As a result, the penetration depth of the second cutter is irregular during cutting, causing a discontinuity of the cutting force chain of the second cutter. In summary, the dominant surface contact force of the rock is pressure as the cutter is breaking the rock, whereas the internal contact force of the rock is primarily tension, and the two cutters influence each other.

The normal force and tangential force of the cutters with different penetration depths and different cutter spacings are shown in Figure 18. We show the average

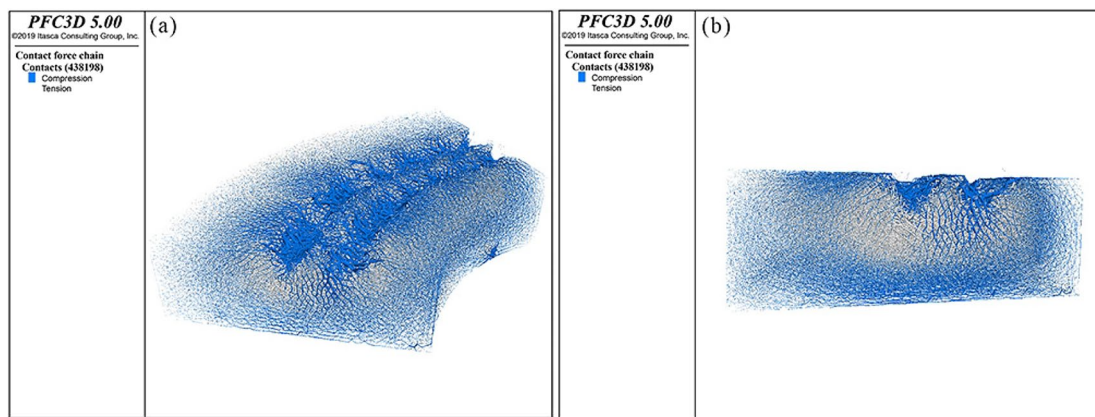


**Figure 17** Rock contact force chain diagram: **a** Top view of contact force chain, and **b** Side view of contact force chain

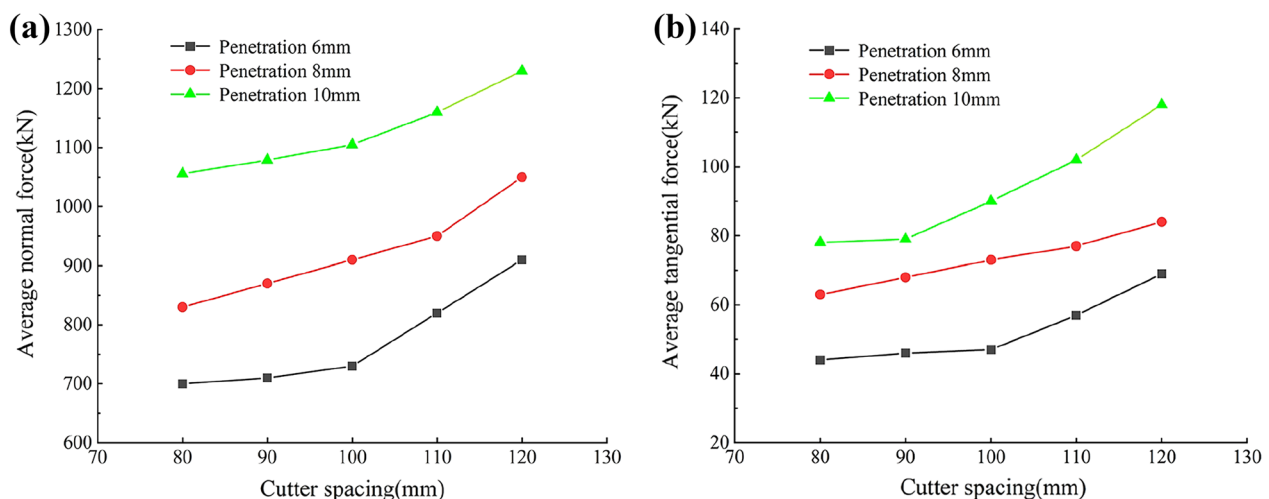


**Figure 18** Average force change graph of two disc cutter at the end of rock breaking with 2 # disc cutter: **a** Average normal force of disc cutter, and **b** Average tangential force of disc cutter

values of the normal force and tangential force of the two cutters.

The average normal force of the cutter increases with an increase in the cutter spacing for the same penetration depth. The force increases slowly initially, followed by a more rapid increase after reaching a critical point. The reason is the change in the rock-breaking area, as described above. The rock-breaking areas of the two cutters overlap, affecting the connection of the rock particles near the rock-breaking track of the #2 cutter. As a result, the cutter can more easily break the nearby rock, resulting in a lower normal force of this cutter. The changes in the average tangential force of the cutter are similar to those of the average normal force.

#### 4.4.2 Force Analysis of Wedge Tooth Cutter

The tangential force and normal force of the wedge tooth cutter are shown in Figure 19. The two forces of the #1 and #2 wedge tooth cutters fluctuate during rock breaking, and their trends are similar to those of the disc cutter. The normal force of the two kinds of the cutter is obviously larger than the tangential force, indicating that the positive impact of the cutter on the rock is greater in the process of rock breaking. Because of the structure of the wedge tooth, there is the characteristic of a rock impact, and the impact force on the front of the rock is stronger, so the normal force of the wedge tooth cutter is obviously larger than that of the disc cutter.

Figure 20 shows the top view of the contact force chain. The contact force chain between the rock particles is

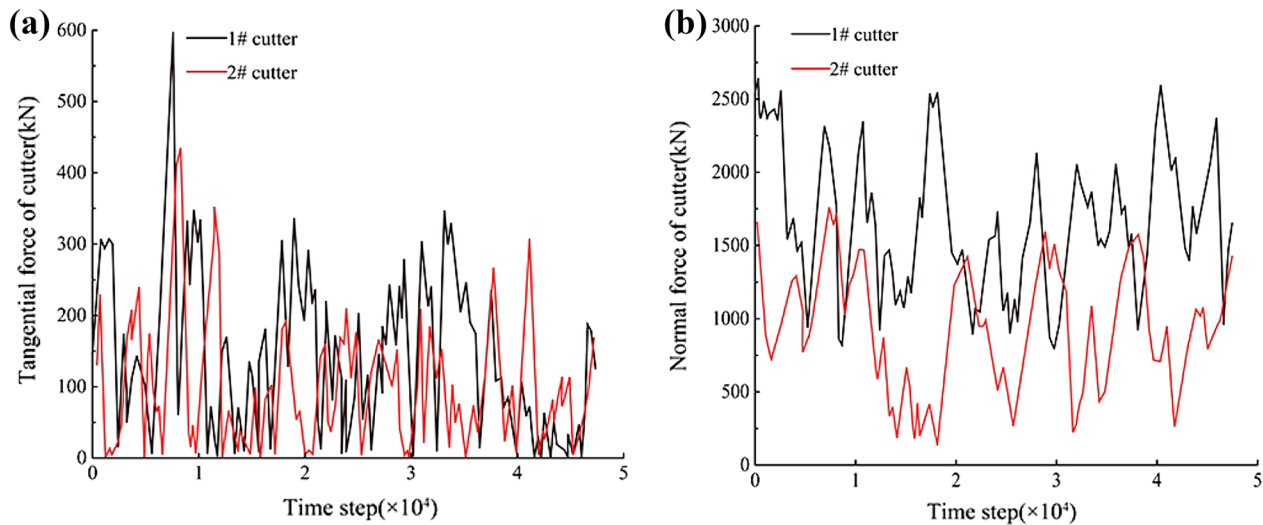


**Figure 19** Force change diagram of wedge tooth cutter: **a** Variation diagram of tangential force of cutter, and **b** Variation diagram of normal force of cutter

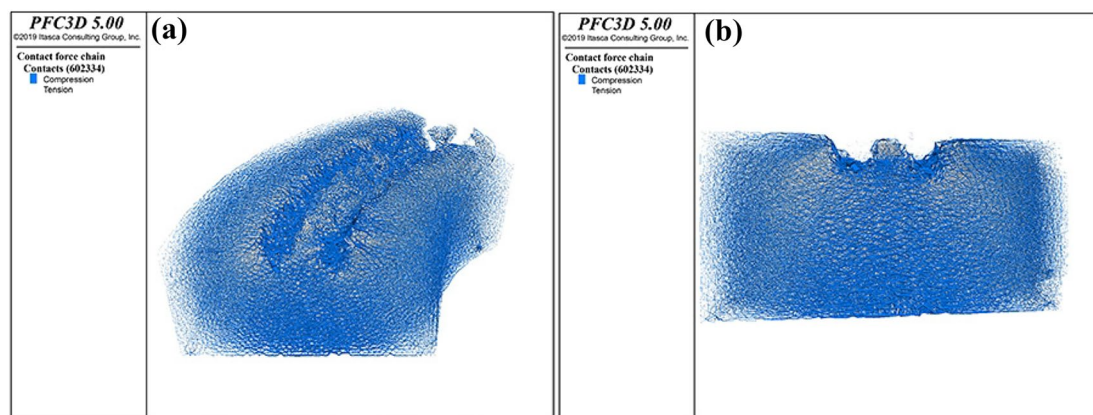


**Figure 20** Rock contact force chain diagram: **a** Top view of contact force chain, and **b** Side view of contact force chain

broken at the end of the rock cutting track due to the large breaking range of the detached area. The connection between many particles is broken; thus, the rock-breaking efficiency is higher than that of the disc cutter. Since the number of rock particles is not the same for the wedge tooth cutter and the disc cutter, we cannot compare the number of contact force chains. However, the particle density per unit volume of the rock is the same. The color of the two contact forces is darker for the wedge tooth cutter than for the disc cutter; therefore, the density of the two forces is higher for the former than for the latter. These results indicate that the destructive force of the wedge tooth cutter is greater than that of the disc cutter under the same conditions.

The normal force and tangential force of the cutters with different penetration depths and different cutter spacings are shown in Fig. 21. We show the average values of the normal force and tangential force of the two cutters. In summary, the trends of the two forces are similar for the wedge tooth cutter and disc cutter, but the numerical values of the forces are larger for the former than for the latter.

#### 4.5 Analysis of the Specific Energy of Rock Breaking

The rock-breaking specific energy refers to the energy consumed by the shield machine to break the rock per unit volume during tunneling. This index is typically used to measure the tunneling energy consumption of shield machines. According to the CSM stress prediction model [36], the rock-breaking specific energy of the cutterhead can be expressed by the following equation:

$$E_s = \frac{E}{V} = \frac{F_t h + 2\pi T_q}{\pi R_t^2 h}, \quad (1)$$

where  $E_s$  is the specific energy of rock breaking, MJ/m<sup>3</sup>;  $E$  is the energy consumed by the rotating shield cutterhead per unit distance during rock breaking, MJ/m<sup>3</sup>;  $V$  is the volume of broken rock per unit distance during rock breaking, m<sup>3</sup>;  $F_t$  is the total thrust of the cutterhead in during shield tunneling, kN;  $h$  is the penetration depth of the cutterhead, m;  $T_q$  is the total torque during shield tunneling, kN·m;  $R_t$  is the diameter of the cutterhead of the shield machine, m.

The rock-breaking specific energy of the cutter is defined as:

$$E_s = \frac{W}{V} = \frac{F_v P + F_r L}{V}, \quad (2)$$

where  $E_s$  is the specific energy of rock breaking, MJ/m<sup>3</sup>;  $W$  is the total energy consumed by the cutter during rock breaking, MJ;  $V$  is the total rock crushing volume of the cutter during rock breaking, m<sup>3</sup>;  $F_v$  is the normal force on the cutter during rock breaking, kN;  $P$  is the penetration depth of the cutter, m;  $F_r$  is the tangential force on the cutter during rock breaking, kN;  $L$  is the cutting distance of the cutter, m.

As the cutter spacing of the disc cutter or wedge tooth cutter increases, the rock-breaking specific energy decreases first and then increases. A minimum cutter spacing exists with the lowest rock-breaking specific energy at a given penetration depth. However, the optimal cutter spacing and optimal penetration depth cannot be determined solely by the specific energy of rock breaking because the rock-breaking specific energy does not

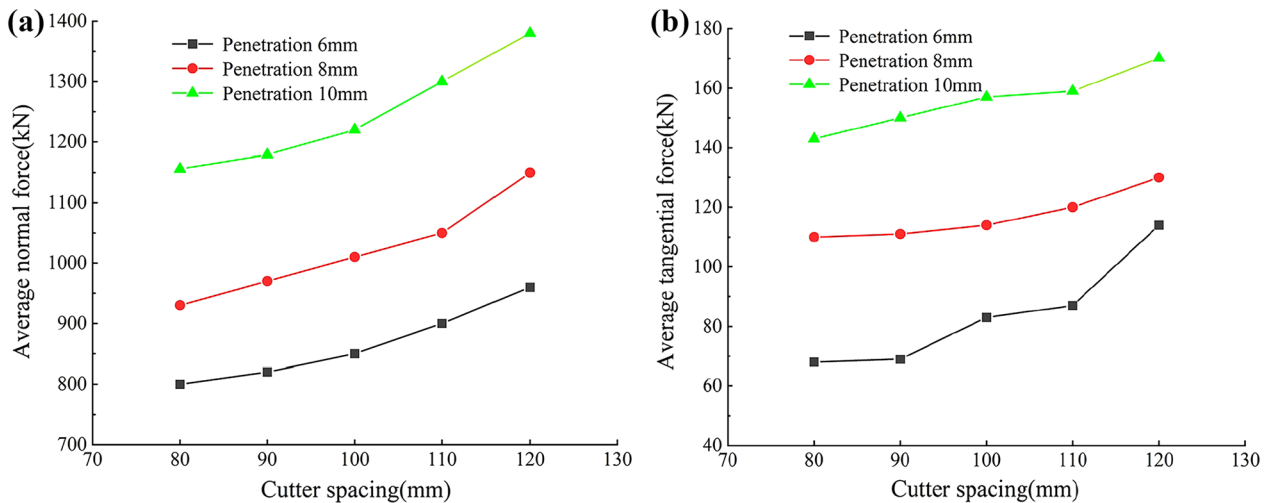


**Figure 21** Average force change graph of two wedge tooth cutter at the end of rock breaking with 2 # wedge tooth cutter: **a** Average normal force of wedge tooth cutter, and **b** Average tangential force of wedge tooth cutter



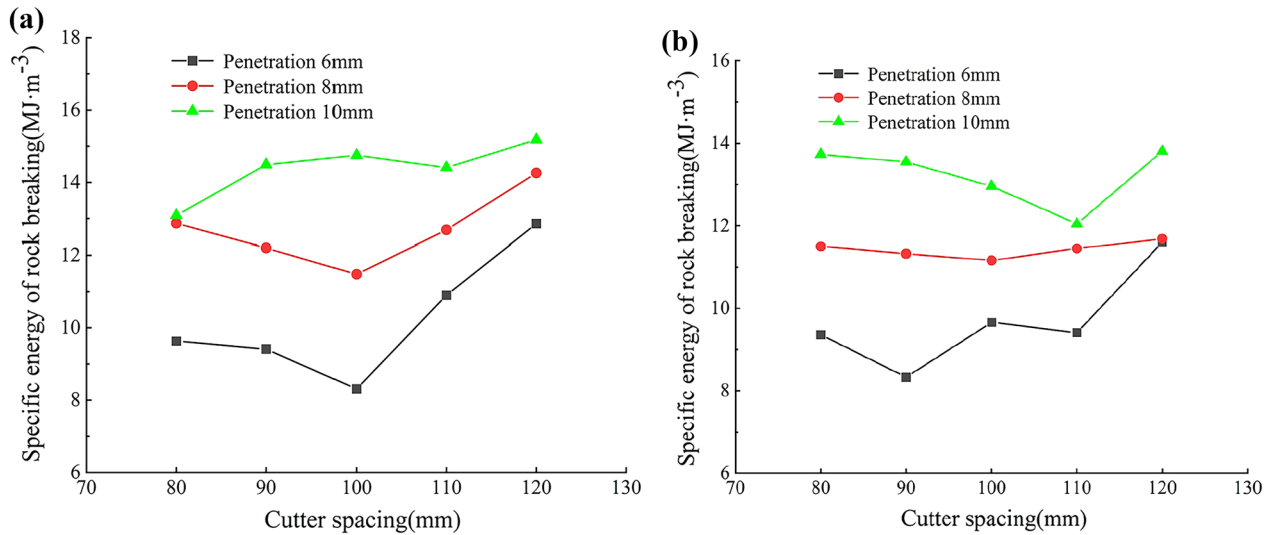


**Figure 22** Change graph of cutter rock-breaking specific energy at the end of rock breaking with 2 # cutter: **a** Specific energy variation diagram of disc cutter, and **b** Specific energy variation diagram of wedge tooth cutter

determine the degree of rock fragmentation (for example, when the rock-breaking specific energy is low, the number of rock cracks is very small). Therefore, it is necessary to consider the rock-breaking conditions and the rock-breaking specific energy to determine the optimal cutter spacing and penetration depth. Figure 22 shows the relationship between the number of cracks and the specific energy of rock breaking of the disc cutter and wedge tooth cutter.

The fifteen experimental schemes were divided into three groups according to the penetration depth. One

scheme in each group has the lowest specific energy (A, B, C). We refer to the three schemes A, B, and C as the optimal schemes at the corresponding penetration depth. We connected points A, B, and C and found that the slope  $K$  of the broken line represents the specific energy required to increase the number of cracks per unit value. Therefore, the smaller the slope, the lower the specific energy consumption of increasing the number of cracks is, and the higher the rock-breaking efficiency is and vice versa.

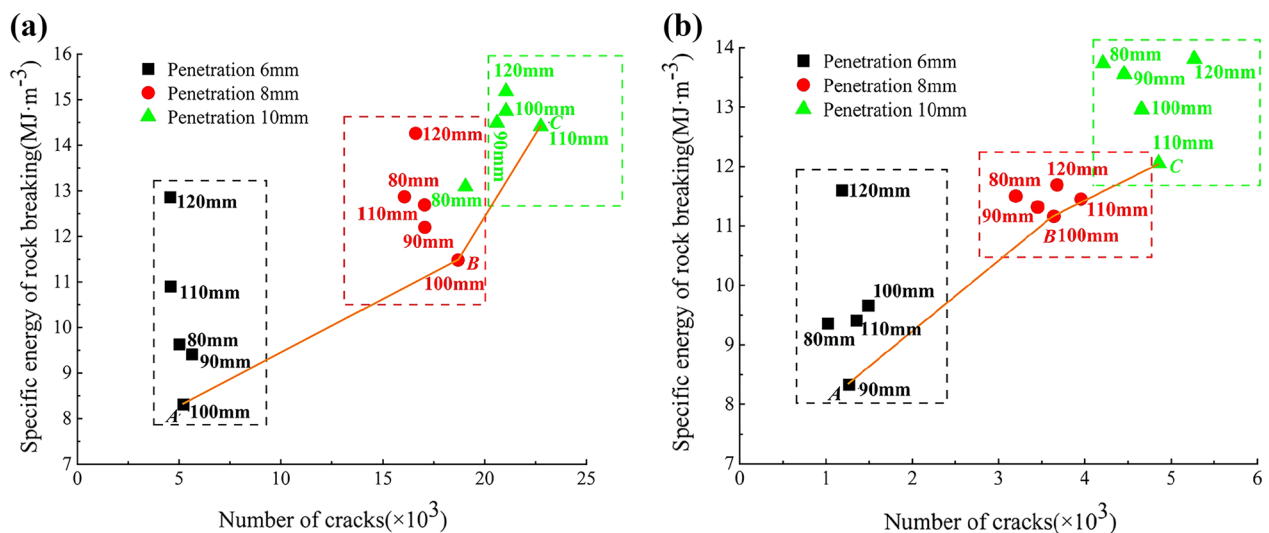


**Figure 23** Relationship between specific energy and crack number of the cutter: **a** Relationship between specific energy and crack number of the disc cutter, **b** Relationship between specific energy and crack number of the wedge tooth cutter

Therefore, we draw the following conclusions: in Figure 23(a), the slope of  $AB$  is less than that of  $BC$ , so the rock-breaking efficiency is equal at  $A$  and  $B$ , but both are greater than  $C$ , and the number of cracks is much larger at point  $B$  than at point  $A$ . Since the degree of rock fragmentation is much higher at point  $B$  than at point  $A$ , point  $B$  is the optimum scheme, namely a cutter spacing of 100 mm and a penetration depth of 8 mm. Similarly, in Figure 23(b), the slope of  $AB$  is greater than that of  $BC$ , the rock-breaking efficiency of  $A$  and  $B$  are equal, but both are less than  $C$ . The number of cracks at point  $C$  is the largest, indicating that the degree of rock fragmentation is the largest at this point. Thus, point  $C$  is the optimal scheme: a cutter spacing of 110 mm and a penetration depth of 10 mm.

## 5 Conclusions

The rock-breaking process of a disc cutter and wedge tooth cutter were numerically simulated by PFC<sup>3D</sup>, and the rock-breaking specific energy was analyzed theoretically. The following conclusions were obtained:

- (1) The damage caused by the cutter indicated that the rock failure had three stages: the advanced influence, crushing, and stabilizing stages. The #1 cutter partially crushed the rock before the #2 cutter reached the same section. As the second cutter approached this section, the crushing degree increased. Subsequently, the damage to this section stabilized.
- (2) The number of broken particles and cracks per unit rock was about twice as much for the wedge tooth cutter than for the disc cutter under the same conditions. The force chain diagram indicated that the rock damage caused by the wedge tooth cutter was substantially higher than that of the disc cutter.
- (3) The normal force of the two kinds of the cutter is greater than the tangential force, which is because the rock breaking process of the cutter is a positive process. Because the wedge gear cutter tooth block has a periodic impact on the rock in the process of rock breaking, and the impact force is greater than the rolling force of the disc cutter, from the calculation results, the normal force of the wedge tooth cutter is significantly higher than the disc cutter under the same conditions.
- (4) A cutter spacing with the lowest rock-breaking specific energy exists for each penetration depth, but this scheme may not be optimal. At a penetration depth of 6 mm, the rock-breaking specific energy of the disc cutter was slightly lower than that of the wedge tooth cutter. However, as the penetration depth increased further, the rock-breaking specific

energy of the wedge tooth cutter was lower than that of the disc cutter. The optimal rock breaking conditions of the disc cutter (wedge tooth cutter) were a cutter spacing of 100 mm (110 mm) and a penetration depth of 8 mm (10 mm). Therefore, two types of cutters with different penetration depths or cutter spacings should be considered. The number of teeth of the wedge tooth cutter can be increased to improve the rock-breaking efficiency of the shield.

## Acknowledgements

Not applicable.

## Author Contributions

HJ: conceptualization, supervision; HZ: data analysis, writing-original draft; XZ: data analysis and writing-review & editing; YJ: funding acquisition, resources; YZ: data collection in the field, data analysis. All authors read and approved the final manuscript.

## Authors' Information

Hua Jiang, born in 1984, is currently an associate professor at School of Mechanics and Civil Engineering, China University of Mining and Technology Beijing, China.

Huiyan Zhao, born in 1997, is currently a postgraduate at School of Mechanics and Civil Engineering, China University of Mining and Technology Beijing, China.

Xiaoyan Zhang, born in 1986, is currently an associate professor at School of Mechanics and Civil Engineering, China University of Mining and Technology Beijing, China.

Yusheng Jiang, born in 1964, is currently a professor at School of Mechanics and Civil Engineering, China University of Mining and Technology Beijing, China.

Yaofu Zheng, born in 1996, is currently a postgraduate at School of Mechanics and Civil Engineering, China University of Mining and Technology Beijing, China.

## Funding

Supported by National Natural Science Foundation of China (Grant Nos. 51608521, 51809264), Beijing Municipal Major Achievements Transformation and Industrialization Projects of Central Universities (Grant No. ZDZH20141141301), the Fundamental Research Funds for the Central Universities (Grant No. 2023ZKPYLJ06).

## Declarations

## Competing Interests

The authors declare no competing financial interests.

Received: 12 July 2022 Revised: 9 April 2023 Accepted: 14 April 2023

Published online: 13 June 2023

## References

- [1] A Delisio, J Zhao, H H Einstein. Analysis and prediction of TBM performance in blocky rock conditions at the Lotschberg Base Tunnel. *Tunnelling and Underground Space Technology*, 2013, 33: 131-142.
- [2] J Hassanpour, J Rostami, J Zhao. A new hard rock TBM performance prediction model for project planning. *Tunnelling and Underground Space Technology*, 2011, 26(5): 595-603.
- [3] S Yagiz. Utilizing rock mass properties for predicting TBM performance in hard rock condition. *Tunnelling and Underground Space Technology*, 2008, 23(3): 326-339.
- [4] Q M Gong, J Zhao. Development of a rock mass characteristics model for TBM penetration rate prediction. *International Journal of Rock Mechanics and Mining Sciences*, 2009, 46(1): 8-18.

- [5] R Gertsch, L Gertsch, J Rostami. Disc cutting tests in Colorado red granite: Implications for TBM performance prediction. *International Journal of Rock Mechanics and Mining Sciences*, 2007, 44(2): 238-246.
- [6] M Yurdakul. Effect of cutting parameters on consumed power in industrial granite cutting processes performed with the multi-disc block cutter. *International Journal of Rock Mechanics and Mining Sciences*, 2015, 76: 104-111.
- [7] C Balci, D Tumac. Investigation into the effects of different rocks on rock cuttability by a V-type disc cutter. *Tunnelling and Underground Space Technology*, 2012, 30: 183-193.
- [8] J W Cho, S Jeon, H Y Jeong, et al. Evaluation of cutting efficiency during TBM disc cutter excavation within a Korean granitic rock using linear-cutting-machine testing and photogrammetric measurement. *Tunnelling and Underground Space Technology*, 2013, 35: 37-54.
- [9] J V Smith. Assessing the ability of rock masses to support block breakage at the TBM cutter face. *Tunnelling and Underground Space Technology*, 2016, 57: 91-98.
- [10] N Innaurato, C Oggeri, P P Oreste, et al. Experimental and numerical studies on rock breaking with TBM tools under high stress confinement. *Rock Mechanics and Rock Engineering*, 2007, 40(5): 429-451.
- [11] N Innaurato, C Oggeri, P Oreste, et al. Laboratory tests to study the influence of rock stress confinement on the performances of TBM discs in tunnels. *International Journal of Minerals Metallurgy and Materials*, 2011, 18(3): 253-259.
- [12] H Q Yang, J F Liu, B L Liu. Investigation on the cracking character of jointed rock mass beneath TBM disc cutter. *Rock Mechanics and Rock Engineering*, 2018, 51(4): 1263-1277.
- [13] Q B Lin, P Cao, R H Cao. Experimental investigation of jointed rock breaking under a disc cutter with different confining stresses. *Comptes Rendus Mecanique*, 2018, 346(9): 833-843.
- [14] M Entacher, E Schuller, R Galler. Rock failure and crack propagation beneath disc cutters. *Rock Mechanics and Rock Engineering*, 2015, 48(4): 1559-1572.
- [15] T Moon, J Oh. A Study of optimal rock-cutting conditions for hard rock TBM using the discrete element method. *Rock Mechanics and Rock Engineering*, 2012, 45(5): 837-849.
- [16] J Rojek, E Onate, C Labra, et al. Discrete element simulation of rock cutting. *International Journal of Rock Mechanics and Mining Sciences*, 2011, 48(6): 996-1010.
- [17] H Huang, B Lecampion, E Detournay. Discrete element modeling of tool-rock interaction I: rock cutting. *International Journal for Numerical and Analytical Methods in Geomechanics*, 2013, 37(13): 1913-1929.
- [18] M Z Naghadehi, R Mikaeil. Optimization of tunnel boring machine (TBM) disc cutter spacing in jointed hard rock using a distinct element numerical simulation. *Periodica Polytechnica-Civil Engineering*, 2017, 61(1): 56-65.
- [19] Z Q Zhang, K J Zhang, W J Dong, et al. Study of rock-cutting process by disc cutters in mixed ground based on three-dimensional particle flow model. *Rock Mechanics and Rock Engineering*, 2020, 53(8): 3485-3506.
- [20] O Su, N A Akcin. Numerical simulation of rock cutting using the discrete element method. *International Journal of Rock Mechanics and Mining Sciences*, 2011, 48(3): 434-442.
- [21] S O Choi, S J Lee. Numerical study to estimate the cutting power on a disc cutter in jointed rock mass. *KSCE Journal of Civil Engineering*, 2016, 20(1): 440-451.
- [22] Q M Gong, J Zhao, Y Y Jiao. Numerical modeling of the effects of joint orientation on rock fragmentation by TBM cutters. *Tunnelling and Underground Space Technology*, 2005, 20(2): 183-191.
- [23] Q M Gong, Y Y Jiao, J Zhao. Numerical modelling of the effects of joint spacing on rock fragmentation by TBM cutters. *Tunnelling and Underground Space Technology*, 2006, 21(1): 46-55.
- [24] J-W Cho, S Jeon, S-H Yu, et al. Optimum spacing of TBM disc cutters: A numerical simulation using the three-dimensional dynamic fracturing method. *Tunnelling and Underground Space Technology*, 2010, 25(3): 230-244.
- [25] O Acaroglu, L Ozdemir, B Asbury. A fuzzy logic model to predict specific energy requirement for TBM performance prediction. *Tunnelling and Underground Space Technology*, 2008, 23(5): 600-608.
- [26] R Teale. The mechanical excavation of rock-Experiments with roller cutters. *International Journal of Rock Mechanics & Mining Sciences & Geomechanics Abstracts*, 1964, 1(1):63-64.
- [27] M C Jaime, Y N Zhou, J S Lin, et al. Finite element modeling of rock cutting and its fragmentation process. *International Journal of Rock Mechanics and Mining Sciences*, 2015, 80: 137-146.
- [28] X H Zhang, D B Hu, J M Li, et al. Investigation of rock breaking mechanism with TBM cutter under traditional and free-face condition. *Engineering Fracture Mechanics*, 2021, 242.
- [29] M Mohammadnejad, S Dehkhoda, D Fukuda, et al. GPGPU-parallelised hybrid finite-discrete element modelling of rock chipping and fragmentation process in mechanical cutting. *Journal of Rock Mechanics and Geotechnical Engineering*, 2020, 12(2): 310-325.
- [30] Y M Xia, Y C Tian, Q Tan, et al. Side force formation mechanism and change law of TBM center cutter. *Journal of Central South University*, 2016, 23(5): 1115-1122.
- [31] J Rostami. Study of pressure distribution within the crushed zone in the contact area between rock and disc cutters. *International Journal of Rock Mechanics and Mining Sciences*, 2013, 57: 172-186.
- [32] M R Ajamzadeh, V Sarfarazi, H Haeri, et al. The effect of micro parameters of PFC software on the model calibration PFC. *Smart Structures and Systems*, 2018, 22(6): 643-662.
- [33] Z H Xu, Z Y Wang, W Y Wang, et al. An integrated parameter calibration method and sensitivity analysis of microparameters on mechanical behavior of transversely isotropic rocks. *Computers and Geotechnics*, 2022: 142.
- [34] J Q Ren, M Xiao, G Q Liu. Rock macro-meso parameter calibration and optimization based on improved BP algorithm and response surface method in PFC 3D. *Energies*, 2022, 15(17): 6290.
- [35] U Castro-Filgueira, L R Alejano, J Arzua, et al. Sensitivity analysis of the micro-parameters used in a PFC analysis towards the mechanical properties of rocks. *Proceedings of the ISRM European Rock Mechanics Symposium (EUROCK), Ostrava, CZECH REPUBLIC, Jun 20-22, 2017*.
- [36] J Rostami, R Gertsch, L Gertsch. Rock fragmentation by disc cutter: a critical review and an update. *Proceedings of North American Rock Mechanics Symposium*. Toronto, 2002.

**Submit your manuscript to a SpringerOpen<sup>®</sup> journal and benefit from:**

- Convenient online submission
- Rigorous peer review
- Open access: articles freely available online
- High visibility within the field
- Retaining the copyright to your article

---

Submit your next manuscript at ► [springeropen.com](https://www.springeropen.com)